Supporting Information

Kimura *et al*. 10.1073/pnas.0801316105

SI Text

Preparation of Deuterated SMN. Lyophilized SMN was dissolved in D_2O and centrifuged to remove insoluble components. The dissolved SMN was thermally unfolded to fully deuterize the protein and then lyophilized. The lyophilized SMN was again dissolved in D_2O and centrifuged. The protein concentrations were confirmed by measuring the absorption at 277 nm ($\varepsilon_{277} = 1.46 \times 10^4\ M^{-1}\cdot cm^{-1}$) (1). The amount of SMN consumed for the entire measurements was ≈2 g. All pD measurements were made with the pH meter (P260; Beckman) equipped with a glass electrode at room temperature. To correct solvent isotope effect on the glass electrode, the direct pH meter reading was corrected by adding 0.40.

Sample Evaluation. SMN used in this study is the single-chain variant of monellin, which is natively composed of A and B chains (1). In SMN, the two chains were connected at the N-terminal residue of A chain and the C-terminal residue of B chain. Furthermore, Cys-45 was replaced with Ser to prevent the formation of cross-bridged dimer. To confirm that the pH-induced unfolding transition of SMN is fully reversible, we compared the CD spectra of two SMN solutions under the same native conditions (pD 9.4). One solution was prepared by dissolving lyophilized and deuterated SMN into a buffer containing 50 mM glycine (pD 9.4), and the other was obtained by 2-fold dilution of an unfolded SMN solution (pD 13.0) with 100 mM glycine buffer. The IR spectra and far-UV CD spectra of these two solutions were indistinguishable. This rules out the possibility that accumulation of the equilibrium intermediates (I_{eq}s) is caused by an irreversible process. In addition, we previously confirmed the monomeric conformation of SMN throughout its kinetic folding process induced by the pH jump from 13.0 to 9.4 at the protein concentration required for the kinetic IR investigation (1).

Observation of Equilibrium IR spectra. We used a FTIR spectrometer equipped with DTGS detector (FTS-575C; Bio-Rad), which is continuously purged with dry air gas. Interferograms of the samples were acquired at 2 cm^{-1} resolution 512 times and Fourier-transformed with a four-point triangular apodization function. Full deuteration of the amide groups was confirmed by the absence of NH and CNH vibration lines at 1,550 and 3,300 cm^{-1}, respectively, in the FTIR spectra.

Analysis of Equilibrium Transitions. The equilibrium unfolding transitions were analyzed by the global fitting procedure using IGOR (Wavemetrics) based on the following three-step scheme:

$$I = I_U + (I_N - I_{I_{eq2}}) \times \left(\frac{10^{n_1(pK_{a_1}-pH)}}{1+10^{n_1(pK_{a_1}-pH)}}\right) + (I_{I_{eq2}} - I_{I_{eq1}}) \times \left(\frac{10^{n_2(pK_{a_2}-pH)}}{1+10^{n_2(pK_{a_2}-pH)}}\right) + (I_{I_{eq1}} - I_U) \times \left(\frac{10^{n_3(pK_{a_3}-pH)}}{1+10^{n_3(pK_{a_3}-pH)}}\right) \quad [1]$$

For the fitting of the CD titration results, the n values were varied among the integer values. For the fitting of the fluorescence and FTIR results, the n values deduced from the CD results were adopted. All of the pK_a values and the spectra for the intermediates were not fixed.

Time-Resolved IR Measurements. The kinetic IR spectra were obtained by using an IR spectrometer (FTS-575C) and a microscope (UMA-500). These were continuously purged with dry N_2 gas to remove the vapor in the system. The IR light was focused to a spot (100 μm) at the observation channel by a casegrane of the microscope. Progress in the folding reaction was detected by moving the mixer-flow cell assembly to the focusing point of the IR light. Interferograms were acquired at 4 cm^{-1} nominal resolution 64 times and Fourier-transformed to the single-beam spectra with a four-point triangular apodization function by Win-IR (Bio-Rad). The temperature of the solution was monitored by using a thermocouple placed at the exit of the flow cell.

Analysis of Secondary Structure Contents. The secondary structure contents were roughly estimated by evaluating the relative areas of the peaks in the deconvoluted IR spectra. First, the IR spectra were resolution-enhanced to emphasize peaks for different structures because the number of the peaks identified in the second derivative spectra was not sufficient for the reliable fitting. The spectra were self-deconvoluted with a Lorentzian band shape of 15 cm^{-1} full width at half-height, then smoothed by an apodization with a Bessel function leading to a resolution enhancement factor k of 1.8 by Win-IR software. Next, the deconvoluted spectra were fitted by Gaussian functions, whose number and peak frequencies were determined in the fourth derivative of the original spectra (data not shown) by using IGOR. The frequency, width, and relative area of the peaks obtained by the fitting are listed in Table S2. The frequencies of the peaks for solvated helix, α-helix, and major and minor lines for β-sheet were identical to those identified in the second derivative spectra within 3 cm^{-1}. The frequencies for turns, not apparent in the second derivative spectra, were adopted from the fourth-derivative spectra. Furthermore, we assumed unordered structure at ≈1,644 cm^{-1}. Finally, the relative areas of the peaks in Table S2 were transcribed to Table 1. The areas for the peaks at 1,679–1,687 cm^{-1} (β-sheet), ≈1,654 cm^{-1} (α-helix), 1,636–1,640 cm^{-1} (solvated helix), and 1,623–1,629 cm^{-1} (β-sheet) are directly listed in Table 1. The areas for the turn at 1,660–1,678 cm^{-1} were summed and are listed in the columns of turn in Table 1. The areas for the unordered structure at 1,640–1,648 cm^{-1} were summed and are listed in the corresponding column in Table 1. We stress that the relative areas of the peaks evaluated in this article should be considered rough estimates of the secondary structure contents because the line shape of amide I′ were modulated by a complex mechanism that precludes the quantitative estimation of the contents (2, 3). Furthermore, the absorption cross sections of amide I′ for different conformations are not constant as demonstrated in the larger positive peak in the difference spectra presented in Fig. S3*c*.

1. Konno T (2001) Multistep nucleus formation and a separate subunit contribution of the amyloidgenesis of heat-denatured monellin. *Protein Sci* 10:2093–2101.
2. Barth A, Zscherp C (2002) What vibrations tell us about proteins. *Q Rev Biophys* 35:369–430.
3. Nishiguchi S, Goto Y, Takahashi S (2007) Solvation and desolvation dynamics in apomyoglobin folding monitored by time-resolved infrared spectroscopy. *J Mol Biol* 373:491–502.

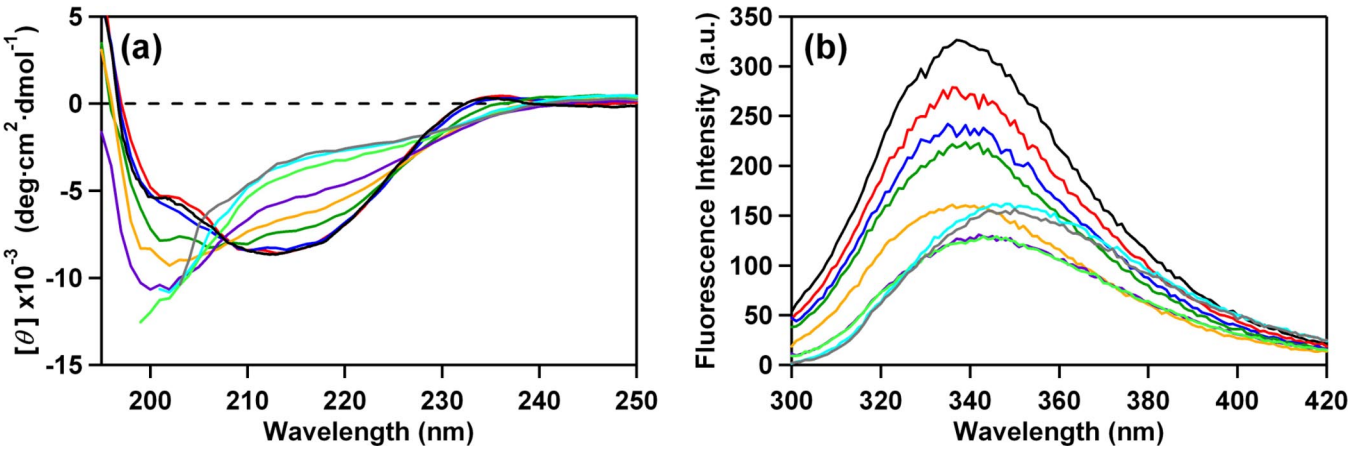

Fig. S1. The equilibrium unfolding transition of SMN at 20°C. (*a*) The alkaline-induced changes of CD spectra. The selected data are presented that were taken at pH 7.1 (black), 9.4 (red), 10.0 (blue), 10.9 (green), 11.0 (orange), 11.1 (purple), 11.6 (light green), 12.0 (light blue), and 13.0 (gray). (*b*) The alkaline-induced changes of Trp fluorescence spectra. The data were taken at pH 9.4 (black), 9.7 (red), 10.0 (blue), 10.3 (green), 10.8 (orange), 11.3 (purple), 11.4 (light green), 11.8 (light blue), and 12.8 (gray).

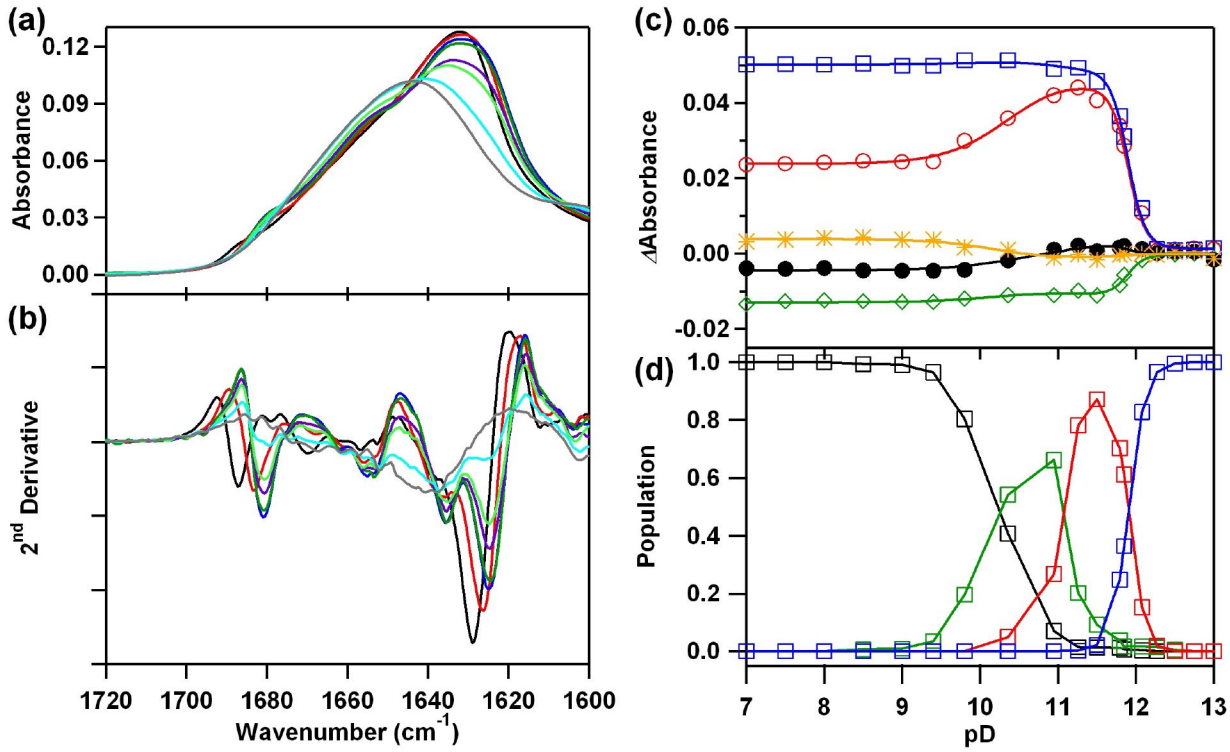

Fig. S2. The equilibrium unfolding transition of SMN at 20°C monitored by FTIR. (*a*) The alkaline induced changes of amide I′ line. The presented spectra were selected from the total of 14 measured spectra and were obtained at pD 9.4 (black), 10.4 (red), 11.2 (blue), 11.5 (green), 11.8 (purple), 11.9 (light green), 12.1 (light blue), and 13.0 (gray). (*b*) The second derivative FTIR spectra of the same titration result. (*c*) Unfolding transition curves monitoring by the difference absorption at wave numbers of 1,621 (red), 1,629 (blue), 1,654 (green), 1,677 (black), and 1,687 (orange) cm^{-1}. Continuous lines are fitting curves based on Eq. **1**. (*d*) pD dependence of the population of each component: N, black; I_{eq2}, green; I_{eq1}, red; U, blue.

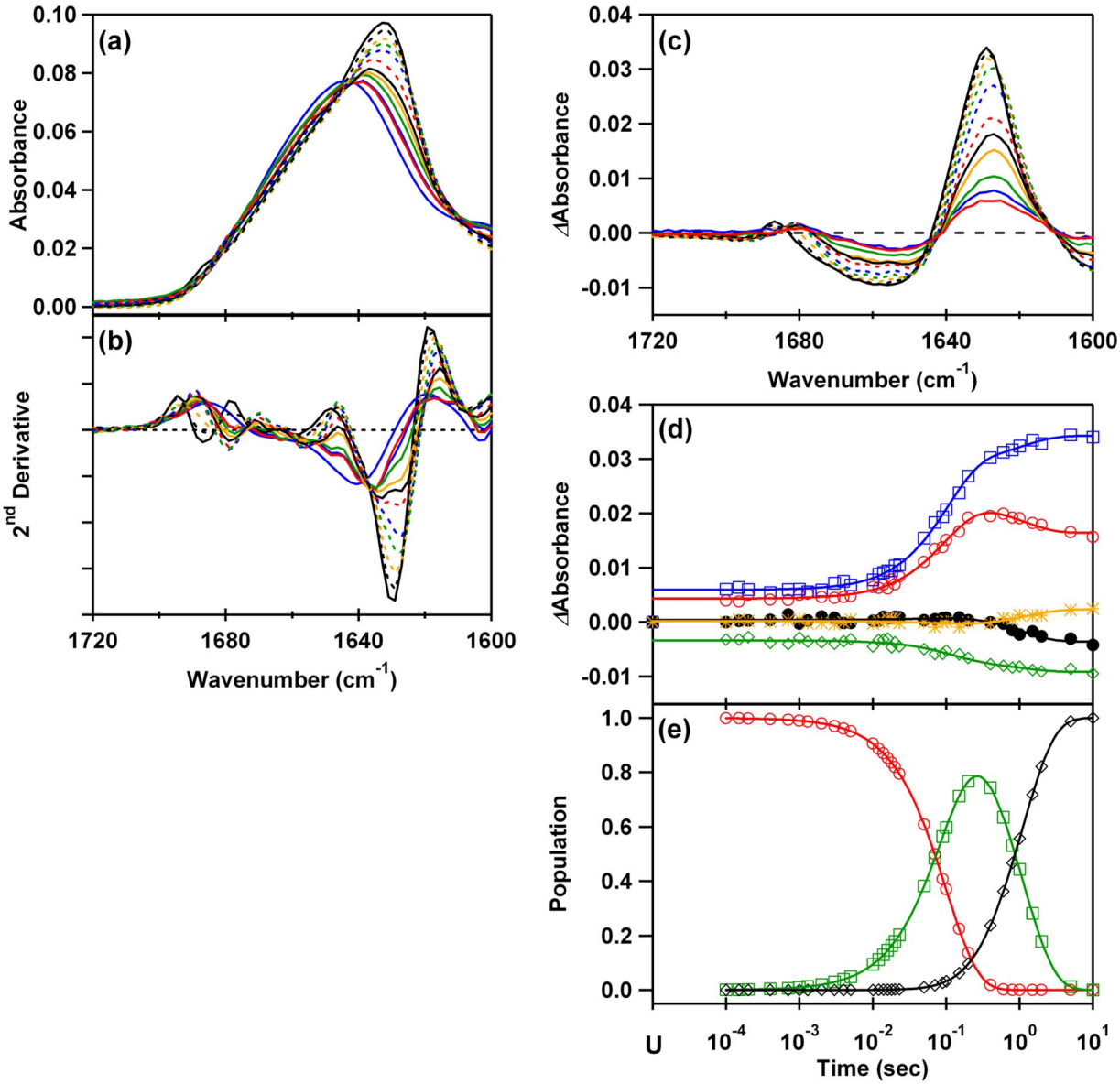

Fig. S3. The time courses of FTIR spectra during the folding of SMN. The kinetic folding of SMN was triggered by pD jump from 13.0 to 9.4 at 25°C. (*a*) The time-resolved amide I′ lines of FTIR spectra. Only 12 of 33 spectra are shown for clarity, corresponding to the initial unfolded state at pD 13.0 (bold blue), the kinetic data at 150 μs (red), 12 ms (blue), 50 ms (green), 90 ms (orange), 100 ms (black), 200 ms (dotted red), 600 ms (dotted blue), 800 ms (dotted green), 2 s (dotted orange), and 10 s (dotted black) after the pD jump, and the native state at pD 9.4 (bold black). (*b*) The second derivative of the same time-resolved data. (*c*) The difference spectra of the same time-resolved data by subtracting the initial unfolded state at pD 13.0. (*d*) Time courses of the changes in the difference absorbance at 1,621 (red), 1,629 (blue), 1,654 (green), 1,677 (black), and 1,687 (orange) cm^{-1}. Continuous lines are predicted curves obtained by fitting the data globally based on the double exponential functions with the rate constants of 10.0 and 0.91 s^{-1}. (*e*) Time courses of the population of each component: I_1, red; I_2, green; N, black.

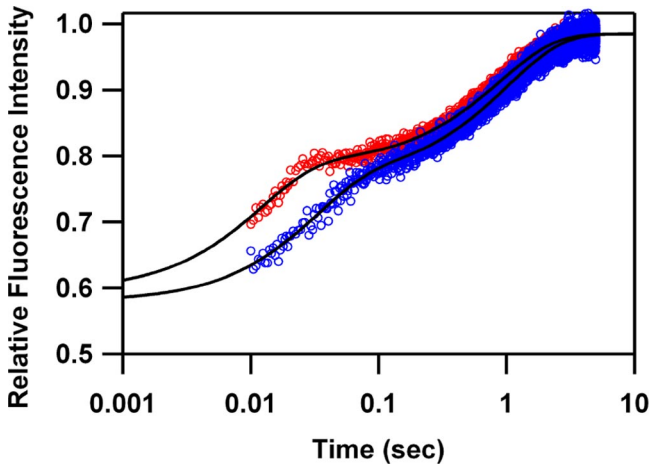

Fig. S4. Time courses of the changes in Trp fluorescence intensity in H_2O (red) and D_2O (blue). The kinetic folding of SMN was triggered by pH or pD jump from 13.0 to 9.4 at 20°C. Continuous lines were obtained by fitting the data based on the double exponential functions with the rate constants of 84.6 and 1.14 s^{-1} in H_2O and 32.4 and 0.99 s^{-1} in D_2O.

Table S1. The pK_a and *n* values for the alkaline unfolding transitions of SMN monitored by CD, tryptophan fluorescence, and FTIR spectroscopies

	N to I_{eq2}		I_{eq2} to I_{eq1}		I_{eq1} to U	
	n_1	pK_{a1}	n_2	pK_{a2}	n_3	pK_{a3}
CD*	1	10.2	5	11.0	4	11.6
Trp fluorescence†	1	10.1	5	11.0	4	11.6
FTIR†	1	10.5	5	11.1	4	11.9

*The pK_a and integer *n* values were obtained by the global fitting of the CD titration results based on the three-step model.

†The pK_a values were obtained by the global fitting of the respective data based on the same model with the fixed *n* values.

Table S2. Assignments of amide I′ components to secondary structures of SMN based on the positive peaks shown in the fourth derivatives

	Wavenumber, cm^{-1} (Content, %; Bandwidth, cm^{-1})						
	Static components				Kinetic components		
Secondary structure	U	I_{eq1}	I_{eq2}	N	I_1	I_2	N
Turn				1,677.7 (7; 11.8)	1,677.2 (12; 12.5)		1,675.3 (3; 10.8)
Turn	1,671.9 (20; 17.8)		1,670.5 (8; 8.9)	1,670.5 (2; 6.9)		1,669.5 (15; 14.3)	1,669.5 (12; 10.8)
Turn	1,662.2 (15; 15.7)	1,664.7 (21; 21.1)	1,667.1 (16; 12.3)	1,660.3 (17; 12.3)	1,665.6 (23; 10.2)	1,663.7 (12; 13.0)	1,661.8 (9; 10.7)
α-Helix		1,653.6 (6; 11.1)	1,654.5 (9; 10.0)	1,653.6 (10; 9.5)		1,654.1 (5; 10.1)	1,654.1 (11; 9.4)
Unordered structures	1,641.0 (65; 21.2)	1,642.5 (21; 14.2)	1,643.9 (18; 11.3)	1,644.9 (16; 10.2)	1,640.6 (48; 19.4), 1,648.3 (6; 11.3)	1,644.4 (19; 9.2)	1,642.5 (15; 9.0)
Solvated helix		1,636.2 (13; 8.2)	1,639.6 (8; 7.0)	1,639.6 (6; 7.0)	1,636.7 (11; 10.3)	1,636.7 (12; 9.9)	1,638.6 (6; 7.1)
β-Sheet							
Major line		1,623.7 (35; 13.2)	1,626.1 (37; 12.0)	1,628.5 (41; 12.0)		1,625.1 (34; 12.5)	1,629.0 (40; 11.1)
Minor line		1,680.1 (5; 5.4)	1,684.4 (4; 5.7)	1,686.9 (2; 4.7)		1,679.1 (3; 5.4)	1,686.8 (2; 4.4)

The assignments are based on the consensus literature data. The secondary structure contents were estimated by Gaussian curve fitting to the resolution-enhanced spectra as described in *SI Text*.